Three-Dimensional Electromagnetics

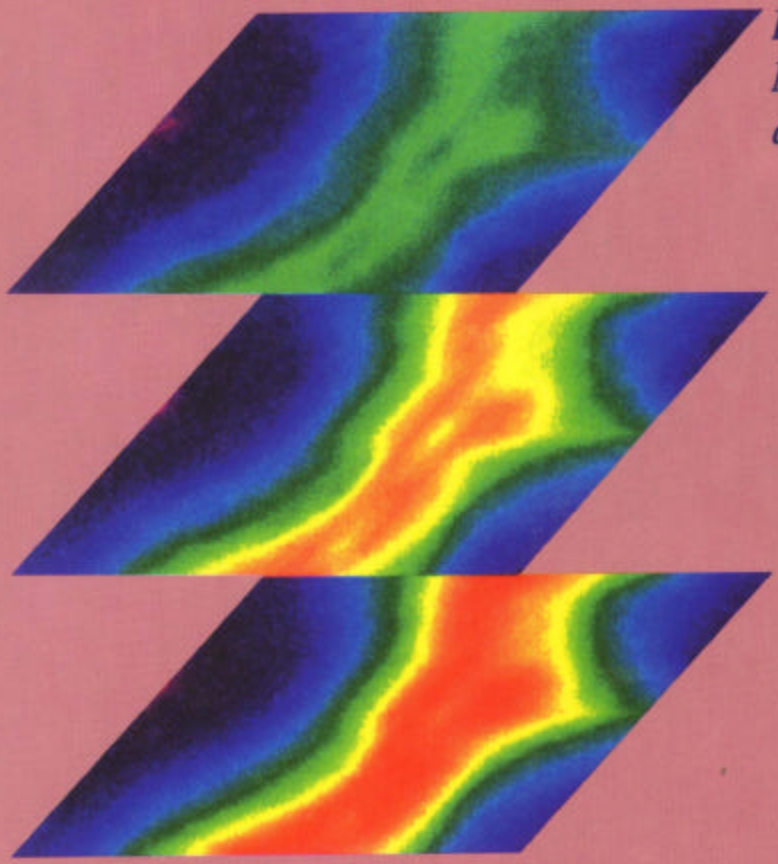

Edited by
Michael Oristaglio
and Brian Spies

Geophysical Developments
No. 7

A New Algorithm for 3-D Nonlinear Electromagnetic Inversion

Ganquan Xie
Jianhua Li

Summary. We propose a new algorithm for 3-D electromagnetic inversion that works with the magnetic-field integral equation (instead of the traditional electric-field integral equation). The forward and inverse integral equations are discretized by the finite element method; solution of the matrix system involves alternating conjugate-gradient and biconjugate-gradient iterations. The solution is regularized by a novel external annealing technique. A coupled-domain decomposition allows a very efficient (96%) implementation of the algorithm on massively parallel machines. Tests on both synthetic and field data from environmental sites yield good subsurface images in a reasonable amount of computational time.

1 Introduction

The distribution of electrical conductivity in the Earth is important in geophysical exploration, oil reservoir management, and environmental site characterization, because the conductivity often is determined mainly by the pore fluids, porosity, and saturation of the rocks. Three-dimensional inversion of electromagnetic (EM) data is, however, ill-posed, strongly nonlinear, and computationally demanding. In our work on this problem (Lee et al., 1995; Xie and Lee, 1995; Xie et al., 1995a, 1995b), we have found that use of the EM integral equation for the magnetic field has certain advantages over standard approaches that use the integral equation for the electric field. We outline the reasons here, beginning with a short derivation of the magnetic-field integral equation for forward modeling and recasting the (nonlinear) EM inverse problem in terms of this equation. We then describe a finite-element method for its discretization and an efficient parallel algorithm for its solution. We conclude with sample inversions of synthetic and field data.

2 Magnetic-field integral equation

Maxwell's equations

$$\nabla \times \mathbf{E} = -i\omega\mu(\mathbf{H} + \mathbf{M}) \tag{1}$$

Earth Sciences Division, Bldg. 90, Lawrence Berkeley National Laboratory, 1 Cyclotron Road, Berkeley, CA 94720, USA.

and

$$\nabla \times \mathbf{H} = (\sigma + i\omega\epsilon)\mathbf{E} + \mathbf{J} \tag{2}$$

allow derivation of integral equations for both the electric and the magnetic fields (Habashy et al., 1993; Torres-Verdin and Habashy, 1994). The more familiar electric-field integral equation is

$$\mathbf{E}(\mathbf{r}) = \mathbf{E}_b(\mathbf{r}) - i\omega\mu \int_{V_s} \mathbf{G}_b^E(\mathbf{r}, \mathbf{r}')[(\sigma - \sigma_b) + i\omega(\epsilon - \epsilon_b)]\mathbf{E}(\mathbf{r}')\, d\mathbf{r}'. \tag{3}$$

The different quantities are defined in the standard way: $\mathbf{E}$ is the total electric field; $\mathbf{E}_b$ is the background electric field; $\mathbf{H}$ is the total magnetic field; μ is the magnetic permeability; σ is the electric conductivity; ϵ is the electric permittivity; ω is the (angular) frequency; σ_b is the background electric conductivity; ϵ_b is the background electric permittivity; $\mathbf{J}$ is an electric current source; $\mathbf{M}$ is a magnetic current source; points $\mathbf{r}$ and $\mathbf{r}'$ are in the domain V_s, where $\sigma - \sigma_b + i\omega(\epsilon - \epsilon_b) \neq 0$; finally, $\mathbf{G}_b^E(\mathbf{r}, \mathbf{r}')$ is the Green dyadic for the electric field in the background medium. In a layered medium, the Green dyadic can be split into a whole-space part and a contribution from the layering:

$$\mathbf{G}_b^E(\mathbf{r}, \mathbf{r}') = \left(I + \frac{1}{k_b^2}\nabla\nabla\right) g_b(\mathbf{r}, \mathbf{r}') + \mathbf{G}_s^E(\mathbf{r}, \mathbf{r}'), \tag{4}$$

where

$$g_b(\mathbf{r}, \mathbf{r}') = \frac{e^{-ik_b|\mathbf{r}-\mathbf{r}'|}}{4\pi|\mathbf{r} - \mathbf{r}'|}; \tag{5}$$

$$k_b^2 = -i\omega\mu(\sigma_b + i\omega\epsilon_b), \tag{6}$$

$$|\mathbf{r} - \mathbf{r}'| = \sqrt{(x - x')^2 + (y - y')^2 + (z - z')^2}. \tag{7}$$

Taking $\nabla\times$ on both sides of Eq. (3) and using the second of Maxwell's equations gives the following integral equation for the magnetic field:

$$\begin{aligned}\mathbf{H}(\mathbf{r}) = \mathbf{H}_b(\mathbf{r}) &- \int_{V_s} \nabla_{r'} g_b(\mathbf{r}, \mathbf{r}') \times \frac{(\sigma - \sigma_b) + i\omega(\epsilon - \epsilon_b)}{\sigma + i\omega\epsilon}(\nabla_{r'} \times \mathbf{H} - \mathbf{J})\, d\mathbf{r}' \\ &+ \int_{V_s} \nabla_r \times \mathbf{G}_s^E(\mathbf{r}, \mathbf{r}') \frac{(\sigma - \sigma_b) + i\omega(\epsilon - \epsilon_b)}{\sigma + i\omega\epsilon}(\nabla_{r'} \times \mathbf{H} - \mathbf{J})\, d\mathbf{r}',\end{aligned} \tag{8}$$

where $\mathbf{H}_b$ is the background magnetic field, ∇_r is the gradient in variable $\mathbf{r}$, and $\nabla_{r'}$ is the gradient in variable $\mathbf{r}'$. The magnetic and electric integral equations are equivalent theoretically, but not numerically. The advantages of the integral equation (8) is described in Section 8.

3 New nonlinear EM inversion using integral equations

EM inversion amounts to solving the following nonlinear Fredholm integral equation of the first kind:

$$\begin{aligned}\mathbf{H}_d(\mathbf{r}) = \mathbf{H}_b(\mathbf{r}) &- \int_{V_s} \nabla_{r'} g_b(\mathbf{r}, \mathbf{r}') \times \frac{(\sigma - \sigma_b) + i\omega(\epsilon - \epsilon_b)}{\sigma + i\omega\epsilon}(\nabla_{r'} \times \mathbf{H} - \mathbf{J})\, d\mathbf{r}' \\ &+ \int_{V_s} \nabla_r \times \mathbf{G}_s^E(\mathbf{r}, \mathbf{r}') \frac{(\sigma - \sigma_b) + i\omega(\epsilon - \epsilon_b)}{\sigma + i\omega\epsilon}(\nabla_{r'} \times \mathbf{H} - \mathbf{J})\, d\mathbf{r}',\end{aligned} \tag{9}$$

where $\mathbf{H}_d$ is the measured magnetic-field data; $\mathbf{H}_b$ is the background magnetic field; $\mathbf{H}$ is a magnetic field inside the domain V_s that satisfies the magnetic integral equation (8). Equation (9) is similar to Eq. (8) in form, but is a nonlinear integral equation for the electric conductivity and permittivity in V_s when data are given at points $\mathbf{r}$ outside the domain. The first variation of the nonlinear operator is

$$\begin{aligned}\delta\mathbf{H}(\mathbf{r}) = &\int_{V_s} \nabla_{r'} g_b(\mathbf{r},\mathbf{r}') \times \frac{\delta(\sigma+i\omega\epsilon)}{\sigma+i\omega\epsilon}\frac{(\sigma_b+i\omega\epsilon_b)}{\sigma+i\omega\epsilon}(\nabla_{r'}\times\mathbf{H}-\mathbf{J})\,d\mathbf{r}'\\ &-\int_{V_s}\nabla_r\times\mathbf{G}_s^E(\mathbf{r},\mathbf{r}')\frac{\delta(\sigma+i\omega\epsilon)}{\sigma+i\omega\epsilon}\frac{(\sigma_b+i\omega\epsilon_b)}{\sigma+i\omega\epsilon}(\nabla_{r'}\times\mathbf{H}-\mathbf{J})\,d\mathbf{r}'\\ &-\int_{V_s}\nabla_{r'}g_b(\mathbf{r},\mathbf{r}')\times\frac{(\sigma-\sigma_b)+i\omega(\epsilon-\epsilon_b)}{\sigma+i\omega\epsilon}\nabla_{r'}\times\delta\mathbf{H}\,d\mathbf{r}'\\ &+\int_{V_s}\nabla_r\times\mathbf{G}_s^E(\mathbf{r},\mathbf{r}')\frac{(\sigma-\sigma_b)+i\omega(\epsilon-\epsilon_b)}{\sigma+i\omega\epsilon}\nabla_{r'}\times\delta\mathbf{H}\,d\mathbf{r}'. \qquad (10)\end{aligned}$$

Because the nonlinear integral equation (9) is ill-posed, we transform it into the minimization of the following regularized functional:

$$\begin{aligned}\sum_{\ell=1}^{n_{fsr}}\Big\|&\mathbf{H}_\ell(\mathbf{r})-\mathbf{H}_{b,\ell}(\mathbf{r})+\int_{V_s}\nabla_{r'}g_b(\mathbf{r},\mathbf{r}')\times\frac{(\sigma-\sigma_b)+i\omega(\epsilon-\epsilon_b)}{\sigma+i\omega\epsilon}(\nabla_{r'}\times\mathbf{H}_\ell-\mathbf{J})\,d\mathbf{r}'\\ &-\int_{V_s}\nabla_r\times\mathbf{G}_s^E(\mathbf{r},\mathbf{r}')\frac{(\sigma-\sigma_b)+i\omega(\epsilon-\epsilon_b)}{\sigma+i\omega\epsilon}(\nabla_{r'}\times\mathbf{H}_\ell-\mathbf{J})\,d\mathbf{r}'\Big\|^2\\ &+\alpha(\mathbf{R}(\sigma+i\omega\epsilon),\sigma-i\omega\epsilon)=\min! \qquad (11)\end{aligned}$$

where $n_{fsr}=n_f\times n_s\times n_r$; n_f is the number of frequencies; n_s is the number of sources; n_r is the number of receivers; $\mathbf{R}$ is a positive-definite regularizing operator; and α is the regularizing parameter.

We use the modified Gauss-Newton iterative method to solve the minimization problem defined by Eq. (11). Let $\mathbf{J}_\ell$ be the Jacobian operator for Eq. (9) ($\mathbf{J}_\ell$ maps a perturbation in $\sigma+i\omega\epsilon$ to a change in magnetic field $\delta\mathbf{H}$; in discrete form, it is a matrix of partial derivatives),

$$\mathbf{J}_\ell\delta(\sigma+i\omega\epsilon)=\delta\mathbf{H}. \qquad (12)$$

We have

$$\begin{aligned}\left[\mathbf{J}_\ell^T\mathbf{J}_\ell+\alpha\mathbf{R}\right]\delta(\sigma+i\omega\epsilon)=-\mathbf{J}_\ell^T\Bigg[&\mathbf{H}_\ell(\mathbf{r})-\mathbf{H}_{b,\ell}(\mathbf{r})+\int_{V_s}\nabla_{r'}g(\mathbf{r},\mathbf{r}')\\ &\times\frac{(\sigma-\sigma_b)+i\omega(\epsilon-\epsilon_b)}{\sigma+i\omega\epsilon}(\nabla_{r'}\times\mathbf{H}_\ell-\mathbf{J})\,d\mathbf{r}'\\ &-\int_{V_s}\nabla_r\times\mathbf{G}_s^E(\mathbf{r},\mathbf{r}')\frac{(\sigma-\sigma_b)+i\omega(\epsilon-\epsilon_b)}{\sigma+i\omega\epsilon}\\ &\times(\nabla_{r'}\times\mathbf{H}_\ell-\mathbf{J})\,d\mathbf{r}'\Bigg]-\alpha\mathbf{R}(\sigma+i\omega\epsilon). \qquad (13)\end{aligned}$$

4 Regularizing method

4.1 External regularizing method

The regularizing operator $\mathbf{R}$ (Tikhonov and Arsenin, 1977) is a positive-definite operator; for example, $\mathbf{R} = -\Delta$, where Δ is the Laplacian operator. This external regularizing approach is easy to construct, but the optimum regularizing parameter α is difficult to select. Let

$$\|\mathbf{H}_{\text{data}} - \mathbf{H}_{\text{model}}\|^2 = \sum_{\ell=1}^{N_{fw}} \Big\| \mathbf{H}_\ell(\mathbf{r}) - \mathbf{H}_{b,\ell}(\mathbf{r}) + \int_{V_s} \nabla_{r'} g_b(\mathbf{r}, \mathbf{r}') \times \frac{(\sigma - \sigma_b) + i\omega(\epsilon - \epsilon_b)}{\sigma + i\omega\epsilon} (\nabla_{r'} \times \mathbf{H}_\ell - \mathbf{J})\, d\mathbf{r}' - \int_{V_s} \nabla_r \times \mathbf{G}_s^E(\mathbf{r}, \mathbf{r}') \frac{(\sigma - \sigma_b) + i\omega(\epsilon - \epsilon_b)}{\sigma + i\omega\epsilon} (\nabla_{r'} \times \mathbf{H}_\ell - \mathbf{J})\, d\mathbf{r}' \Big\|^2. \tag{14}$$

The optimization (11) will be

$$\|\mathbf{H}_{\text{data}} - \mathbf{H}_{\text{model}}\|^2 + \alpha(\mathbf{R}(\sigma + i\omega\epsilon), \sigma - i\omega\epsilon) = \min! \tag{15}$$

Let $\mathbf{H}_e$ be the exact data and

$$\|\mathbf{H}_e - \mathbf{H}_{\text{data}}\| \le \delta, \tag{16}$$

$$f(\alpha) = \|\mathbf{H}_{\text{data}} - \mathbf{H}_{\text{model}}\|^2, \tag{17}$$

$$g(\alpha) = (\mathbf{R}(\sigma + i\omega\epsilon), \sigma - i\omega\epsilon), \tag{18}$$

$$h(\alpha) = \|\mathbf{H}_{\text{data}} - \mathbf{H}_{\text{model}}\|^2 - \delta^2. \tag{19}$$

It can be proved that $f(\alpha)$ is a continuous and almost monotonic nondecreasing function, $g(\alpha)$ is a continuous and almost monotonic nonincreasing function of α, and $h(\alpha)$ is a continuous and almost monotonic function. When $\mathbf{R} = \mathbf{I}$, Yagola (1980) proved a similar result. The minimum root of Eq. (19) will be an optimum regularizing parameter. Xie et al. (1987) proved that the regularized solution is convergent when α goes to zero.

In nonlinear 3-D EM inversion for practical data, δ can only be estimated crudely because it includes physical system data noise and numerical operator error, etc. Therefore, Eq. (19) is solved approximately. We used a local annealing regularizing process to modify the global discrepancy approach. The data-noise preestimation is very important for the inverse problem. For given noise bound δ, because the discrepancy function $h(\alpha)$ is continuous and almost monotonic, we use the quasi-Newton and bisection mixed method to find the optimum regularizing parameter. We also use the bisection method to estimate the error bound δ.

4.2 Internal regularizing method

We used two internal regularizing approaches to solve the nonlinear magnetic integral equation.

4.2.1 High-order variation operator. From the variational operator formula (10), we can obtain first-, second-, and higher-order approximate variational

operators:

$$\delta^{(1)}\mathbf{H}(\mathbf{r}) = -\int_{V_s} \nabla_{r'} g_b(\mathbf{r},\mathbf{r}') \times \frac{\delta(\sigma+i\omega\epsilon)}{\sigma+i\omega\epsilon}\frac{(\sigma_b+i\omega\epsilon_b)}{\sigma+i\omega\epsilon}(\nabla_{r'}\times\mathbf{H}-\mathbf{J})\,d\mathbf{r}' + \int_{V_s} \nabla_r \times \mathbf{G}_s^E(\mathbf{r},\mathbf{r}')\frac{\delta(\sigma+i\omega\epsilon)}{\sigma+i\omega\epsilon}\frac{(\sigma_b+i\omega\epsilon_b)}{\sigma+i\omega\epsilon}(\nabla_{r'}\times\mathbf{H}-\mathbf{J})\,d\mathbf{r}', \tag{20}$$

and

$$\begin{aligned}\delta^{(2)}\mathbf{H}(r) = &-\int_{V_s} \nabla_{r'} g_b(\mathbf{r},\mathbf{r}') \times \frac{\delta(\sigma+i\omega\epsilon)}{\sigma+i\omega\epsilon}\frac{(\sigma_b+i\omega\epsilon_b)}{\sigma+i\omega\epsilon}(\nabla_{r'}\times\mathbf{H}-\mathbf{J})\,d\mathbf{r}' \\ &+\int_{V_s} \nabla_r \times \mathbf{G}_s^E(\mathbf{r},\mathbf{r}')\frac{\delta(\sigma+i\omega\epsilon)}{\sigma+i\omega\epsilon}\frac{(\sigma_b+i\omega\epsilon_b)}{\sigma+i\omega\epsilon}(\nabla_{r'}\times\mathbf{H}-\mathbf{J})\,d\mathbf{r}' \\ &-\int_{V_s} \nabla_{r'} g_b(\mathbf{r},\mathbf{r}') \times \frac{(\sigma-\sigma_b)+i\omega(\epsilon-\epsilon_b)}{\sigma+i\omega\epsilon}\nabla_{r'}\times\delta^{(1)}\mathbf{H}\,d\mathbf{r}' \\ &+\int_{V_s} \nabla_r \times \mathbf{G}_s^E(\mathbf{r},\mathbf{r}')\frac{(\sigma-\sigma_b)+i\omega(\epsilon-\epsilon_b)}{\sigma+i\omega\epsilon}\nabla_{r'}\times\delta^{(1)}\mathbf{H}\,d\mathbf{r}'.\end{aligned} \tag{21}$$

In this nonlinear inversion, $\delta^{(1)}\mathbf{H}$ is used in the first few iterations and then $\delta^{(2)}\mathbf{H}$ is used.

4.2.2 Log-scale approximation

$$\frac{\delta\sigma+i\omega\delta\epsilon}{\sigma+i\omega\epsilon} \cong \delta\log(\sigma+i\omega\epsilon). \tag{22}$$

This formula is a good approximation for low frequency but rough for high frequency. It can be a natural internal regularizing term for high-frequency noise, which is an advantage of using the nonlinear magnetic integral equation (9).

4.3 Annealing regularizing process

There exists a large number of local minima in the nonlinear regularizing magnetic integral optimization (11). In particular, there are accumulative points of the local minimum set because Eq. (11) is ill-posed. The regularizing term can isolate local minima. We use an annealing process to find the global minimum of the regularizing magnetic integral optimization that will provide a high-resolution EM imaging (Xie et al., 1995a, 1995b). Let

$$\begin{aligned}\Delta_1(\sigma+i\omega\epsilon) = \sum_{\ell=1}^{n_{f\omega}} \Big\| &\mathbf{H}_{d,\ell}(\mathbf{r}) - \mathbf{H}_{b,\ell}(\mathbf{r}) \\ &+\int_{V_s} \nabla_r g_b(\mathbf{r},\mathbf{r}) \times \frac{(\sigma-\sigma_b)+i\omega(\epsilon-\epsilon_b)}{\sigma+i\omega\epsilon}(\nabla_r\times\mathbf{H}-\mathbf{J})\,d\mathbf{r} \\ &-\int_{V_s} \nabla_r \times \mathbf{G}_s^E(\mathbf{r},\mathbf{r})\frac{(\sigma-\sigma_b)+i\omega(\epsilon-\epsilon_b)}{\sigma+i\omega\epsilon}(\nabla_r\times\mathbf{H}-\mathbf{J})\,d\mathbf{r}\Big\|^2 \\ &+\alpha(\mathbf{R}(\sigma+i\omega\epsilon),\sigma-i\omega\epsilon),\end{aligned} \tag{23}$$

$$\Delta_2(\sigma+i\omega\epsilon) = A(\sigma+i\omega\epsilon), \tag{24}$$

where A is a positive functional (related to the internal regularizing and constraint conditions); the annealing function is

$$f(\lambda) = e^{-\lambda T}, \tag{25}$$

with decay coefficient λ and pseudotemperature T.

Given an initial $\sigma_0 + i\omega\epsilon_0$ and pseudotemperature T_0, the annealing process is as follows:

1. Perform a quasi-Newton iteration for solving Eqs. (9)–(13) and run a random-process *RAN* simultaneously.
2. Suppose $\sigma_n + i\omega\epsilon_n$ is known and $\delta(\sigma_n + i\omega\epsilon_n)$ is obtained; calculate

$$\begin{aligned}\lambda_n = {} & \Delta_1[\sigma_n + i\omega\epsilon_n + \delta(\sigma_n + i\omega\epsilon_n)] - \Delta_1(\sigma_n + i\omega\epsilon_n) \\ & - \Delta_2[\sigma_n + i\omega\epsilon_n + \delta(\sigma_n + i\omega\epsilon_n)]\end{aligned} \tag{26}$$

3. Update

$$\sigma_{n+1} + i\omega\epsilon_{n+1} = \sigma_n + i\omega\epsilon_n + \delta(\sigma_n + i\omega\epsilon_n) \tag{27}$$

if

$$f(\lambda_n) > RAN. \tag{28}$$

4. Change $T = \mu T_0$, and go back to step 1.

The annealing-regularizing method presented here is robust and is useful for interpreting practical data. The optimum-regularizing parameter cannot be chosen accurately because of noise in practical data. Using the annealing-regularizing method we can, usually obtain reasonable results.

5 Finite-element method

We use the finite-element method to discretize the forward magnetic integral equation (8) and the nonlinear magnetic integral equation (11) (Xie et al., 1995c). The cubic domain is divided into a set of finite cubic block elements. There are eight vertex nodes in each element. Let (x_i, y_i, z_i) be coordinate of the vertex i, and let ℓ, h, and v be the length of the side of the element in the x-, y-, and z-directions, respectively. The trilinear finite-element space $\mathbf{H}^h$ can be constructed with basis functions ϕ_i.

$$\mathbf{H}^h(x, y, z) = \sum_{j=1}^{8} \mathbf{H}_j \phi_j(x, y, z), \tag{29}$$

where

$$\mathbf{H}^h(x, y, z) = \begin{bmatrix} H_x^h(x, y, z) \\ H_y^h(x, y, z) \\ H_z^h(x, y, z) \end{bmatrix}, \tag{30}$$

and

$$\mathbf{H}_j = \begin{pmatrix} H_{xj} \\ H_{yj} \\ H_{zj} \end{pmatrix}. \tag{31}$$

In each cubic element, the basis function is a trilinear function

$$\varphi_i(x, y, z) = \frac{(x - x_i^*)(y - y_i^*)(z - z_i^*)}{(\ell - 2x_i^*)(h - 2y_i^*)(v - 2z_i^*)}, \tag{32}$$

where

$$x_i + x_i^* = \ell, \quad y_i + y_i^* = h, \quad z_i + z_i^* = v, \tag{33}$$

and

$$(x_1, y_1, z_1) = (0, 0, 0), \ldots, (x_8, y_8, z_8) = (0, h, v). \tag{34}$$

Upon substituting Eqs. (29)–(31) and their derivatives into Eq. (8), we obtain the finite-element equation for the discrete magnetic field:

$$\underline{\mathbf{K}}\mathbf{H} = \mathbf{S}. \tag{35}$$

This matrix $\underline{\mathbf{K}}$ is a full matrix, composed of element matrices

$$\underline{\mathbf{K}} = \sum_{e=1}^{M} (\underline{\mathbf{C}}^e)^T \underline{\mathbf{K}}^e \underline{\mathbf{C}}^e \tag{36}$$

where

$$\underline{\mathbf{K}}^e = \left(K_{i,j}^e\right), \quad i, j = 1, 2, \ldots, 8, \tag{37}$$

and $\underline{\mathbf{C}}^e$ is a connection matrix between local and global nodes. Similarly, we can make a finite-element approximation for the nonlinear inverse magnetic integral equation (9) and its derivative operator (20) or (21).

6 Parallel algorithm

We solve the integral equation by a domain-decomposition coupling the global integral equation and a local Galerkin finite-element method. The total numerical-model domain is divided into 2^n subdomains. Two adjacent subdomains should have overlapping strips as in Fig. 1. An algorithm based on finite-element solution or the differential equation for the magnetic field is performed in each subdomain (Xie and Zuo, 1991;

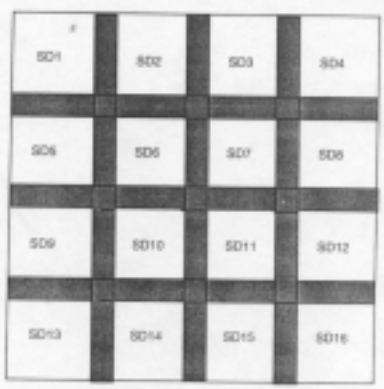

Figure 1. The domain is decomposed into 2^4 subdomains.

Xie et al., 1995c; and Xie et al., 1997) and the integral magnetic forward and inversion algorithm is performed in the overlapping strips. Details of the decomposition method are given in the references. Here we give a brief description. The total discrete matrix is decomposed into 2^n submatrices, each one coupled to its surrounding subdomains. A second-order preconditioned biconjugate (SOR-BCG) iteration is used in parallel to solve the submatrix equations. The 2^n jobs are distributed uniformly into 2^n nodes in a massively parallel computer. A modified first-order global preconditioned biconjugate iteration (PBCG) is used in parallel to solve the reduced global matrix equation. A preconditioned SOR-BCG iteration (Varga, 1962; Wilkinson, 1965; Golub and Van Loan, 1989) is used to solve the inverse integral matrix equation. Note that second-order elements are used in the local subdomain and first-order elements are used in the reduced global iteration. In the 3DEMITINV parallel program, the shared data, shared do loop, and message passing are used to communicate and distribute subdomain field data and matrix data. In this algorithm and parallel program, distribution of the jobs in the parallel processing is uniform and the parallel arrangement is done appropriately. The new domain decomposition approach also has been used for nonlinear integral inversion using Special Parallel Processing (SPP) on the CRAY-A.NERSC.GOV and massively parallel processing (MPP) on the computer T3D.

7 Numerical modeling and inversion

We tested our nonlinear inversion algorithm on two synthetic models. Model 1 is a $90 \times 90 \times 80$ m cubic frame conductor of 0.1 S/m conductivity that includes a $30 \times 30 \times 50$ m cubic conductor of 0.25 S/m conductivity inside (Fig. 2A). The geometry of model 2 is the same as that of model 1; the conductivity in the cubic frame is 0.25 S/m, and the conductivity in the cubic conductor is 0.1 S/m (Fig. 2B). The 18 frequencies (10, 18, 31, 55, 96, 180, 300, 530, 938, 1658, 3000, 5000, 10 000, 16 000, 20 000, 28 000, 38 000, and 50 000 Hz), 64 vertical magnetic dipole sources on the surface, and 768 receivers on the surface were used to make synthetic surface data by solving the forward magnetic integral equation. The geometry of the one source and 12 receivers is shown in Fig. 3. In each receiver point, the three magnetic components, H_x, H_y, and H_z are measured. The amplitude of the vertical magnetic surface data excited by the vertical magnetic source in the center of the surface is shown in Fig. 4 by a solid line; the total field, incident field, and scattered field at 50 000 Hz are shown in plots 1.1, 1.2, and 1.3; the total field, incident field, and scattered field at 10 000 Hz are plotted in 2.1, 2.2, and 2.3; the total field, incident field, and scattered field at 10 Hz are plotted in the 3.1, 3.2, and 3.3. The phase of the vertical magnetic surface data excited by the vertical magnetic source in the center of the surface is shown in Fig. 5 by a solid line. In testing of the inversion, the above model was imbedded in the large cubic domain [−90 m, 90 m; −90 m, 90 m; 0,120 m] and the initial conductivity is 0.05 S/m. After 18 iterations, the conductivity image was obtained. The conductivity imaging of model 1 is shown in (C) of Fig. 2 and the conductivity imaging of model 2 is shown in (D) of Fig. 2. The amplitude and phase of the vertical magnetic field of inversion of the model 1 are shown in Fig. 4 and Fig. 5 by using a dashed line.

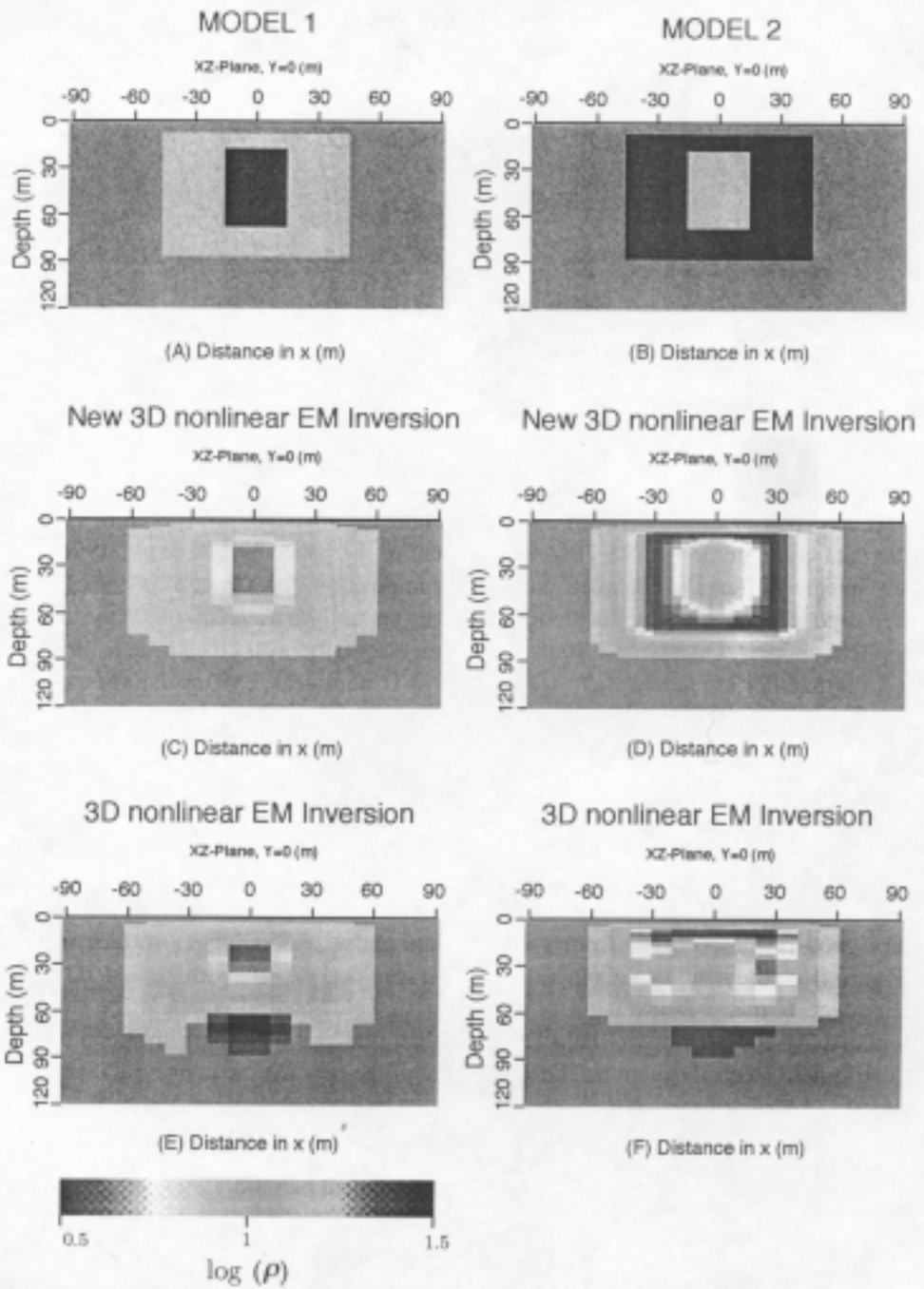

Figure 2. Resistivity imaging of the 3-D EM inversion for synthetic data.

Figure 3. Pattern of the one source and 12 receivers.

For comparison, we used our electric integral inversion program to run the above models and the results are shown in (E) and (F) of Fig. 2. The regularizing parameter of the new inversion is 1.07639X10-5 for model 1, and 78561X10-5 for model 2. We used our new magnetic integral inversion code and electrical integral inversion code to invert VETEM data; the conductivity images are shown in Fig. 6. The data configuration of VETEM is presented in the paper by Lee et al. (1996). A new integral-differential coupled domain decomposition, by Xie et al. (1996c), has been used to parallelize the magnetic integral inversion. We used Cray-C90 to run the synthetic models. On a Cray-C90 using 16 processors, the wall clock time is 30 min, and the parallel efficiency is 96%. The new 3-D nonlinear EM inversion is stable and convergent; its normalized residual reduced to 1.0e-3 from 1.0 after 18 iterations.

8 Conclusion

A new 3-D nonlinear inversion, which works with the magnetic-field integral equation, has been tested on synthetic data and field data from environmental sites. We obtained very good images (Fig. 2) from synthetic data and a reasonable subsurface image (Fig. 6) from the field data. Comparison of the results (Figs. 2C with 2E and 2D with 2F) suggests that 3-D inversion of the magnetic-field integral equation for electric conductivity and permittivity behaves better than (the more familiar) inversion of the electric-field integral equation. The advantages of the new magnetic integral inversion are

1. The magnetic field in Eq. (8) is continuous when electric conductivity is discontinuous, which is convenient for the finite-element method.
2. The kernel function in Eq. (8) is weakly singular.
3. There is a natural internal regularizing term.
4. The integral equation (8) can be used easy to construct a new integral differential coupled parallel domain decomposition.
5. The annealing regularizing for Eq. (8) can be used to find a global minimum of Eq. (11).
6. The magnetic integral equations (8) and (9) are consistent for nonlinear inversion.

Our new algorithm is not suitable for $\omega = 0$. A nonlinear resistivity inversion for direct curent data has been developed by Li et al. (1995).

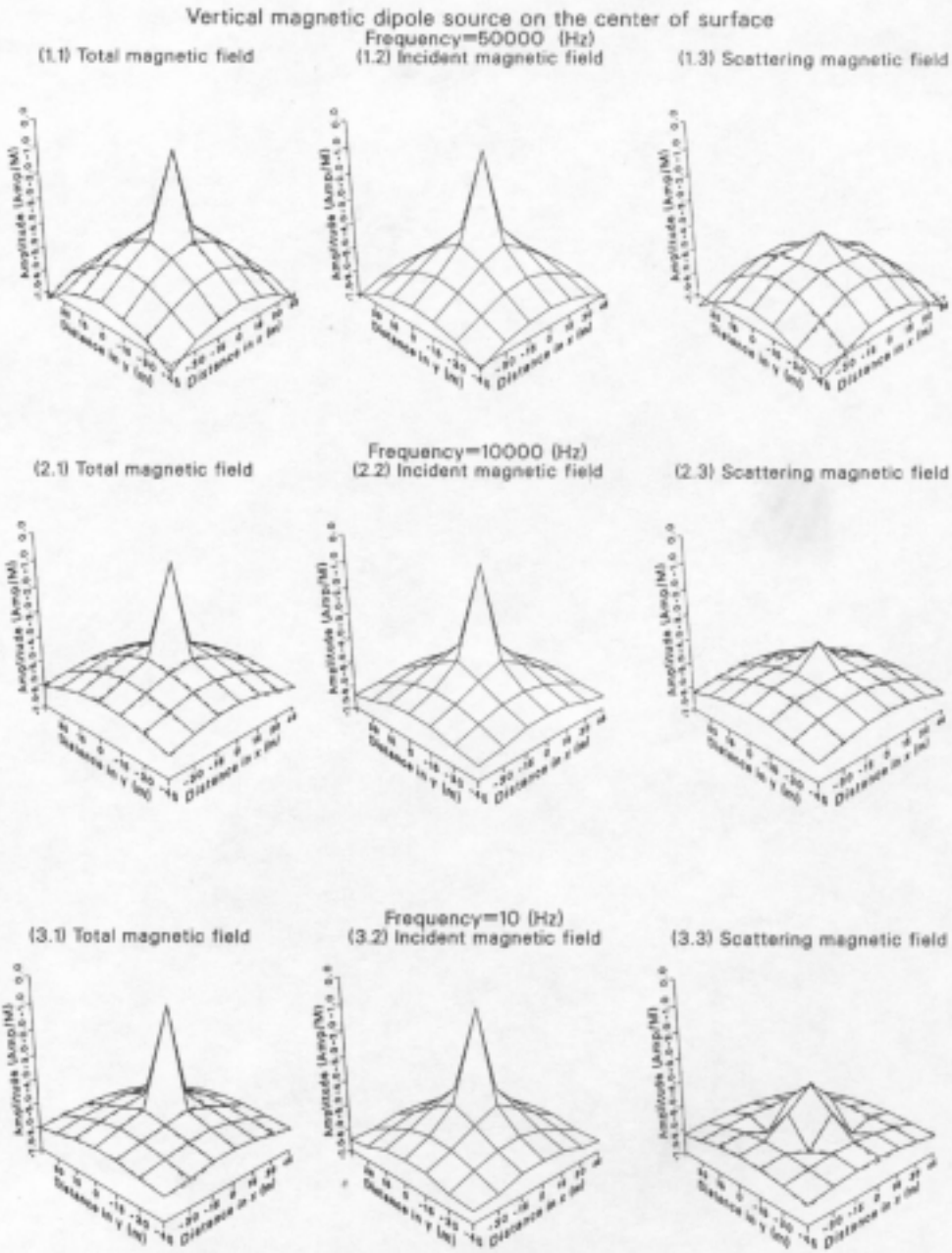

Figure 4. Amplitude of vertical magnetic field on the surface: (solid line) magnetic field of modeling, (dashed line) magnetic field of inversion.

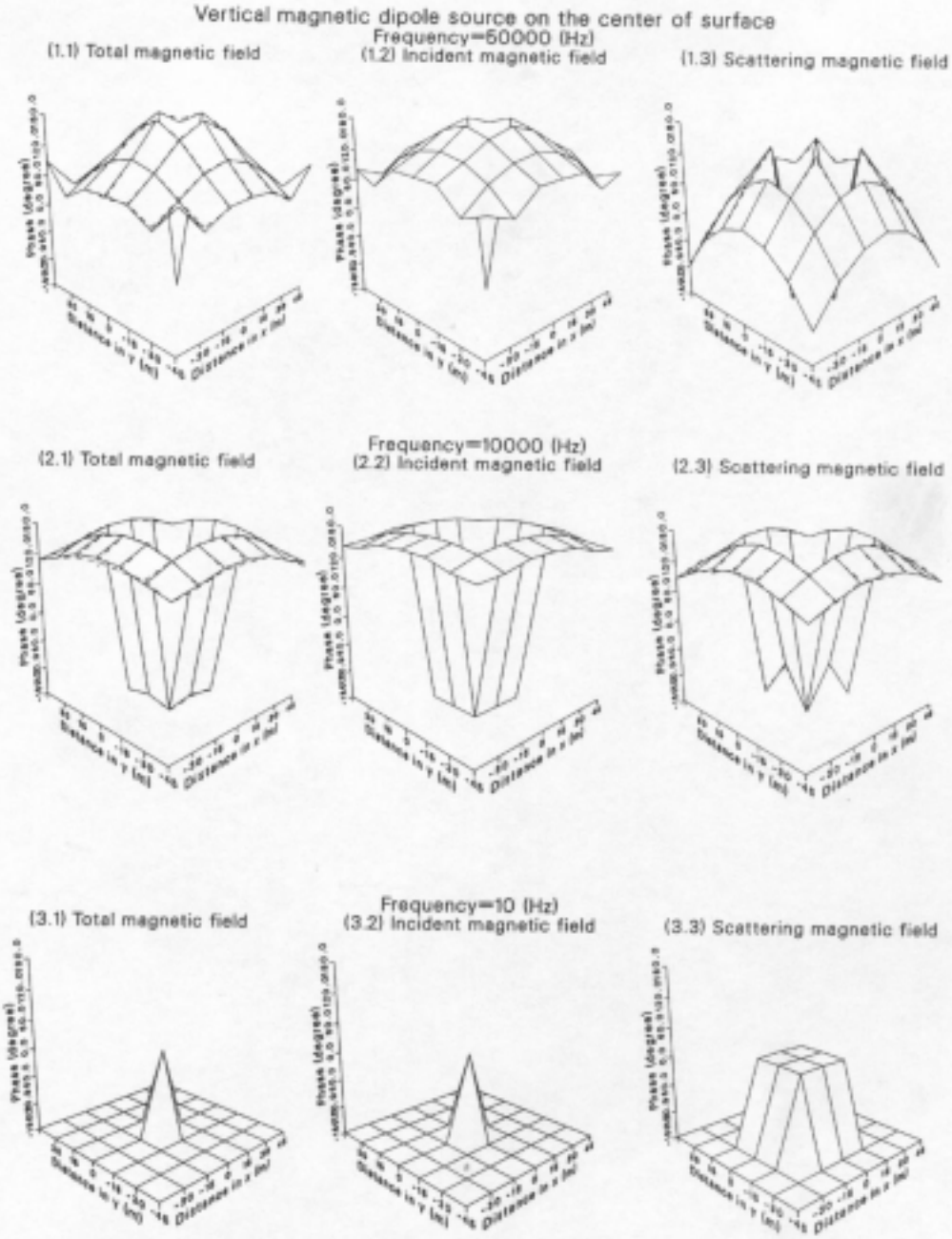

Figure 5. Phase of vertical magnetic field on the surface: (solid line) magnetic field of modeling, (dashed line) magnetic field of inversion.

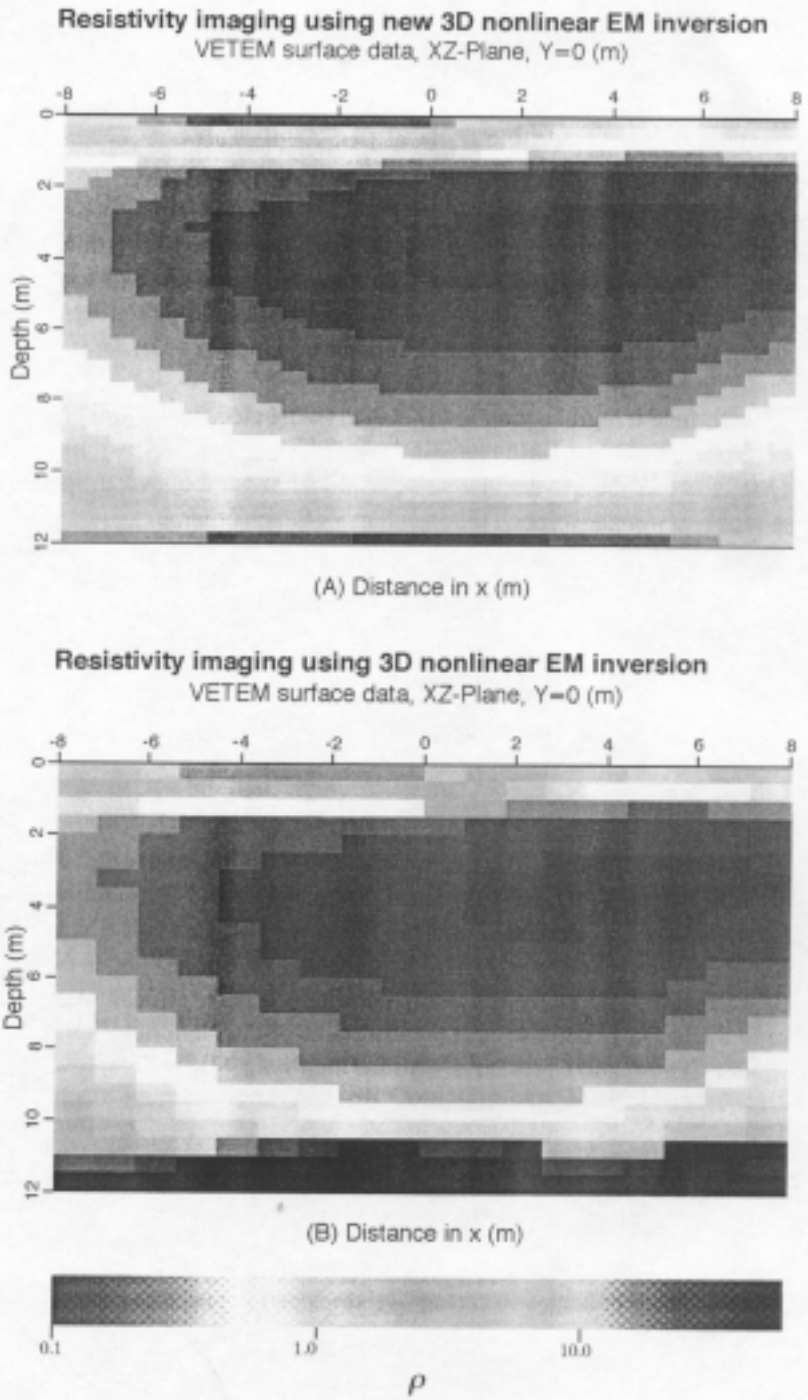

Figure 6. Resistivity imaging of 3-D EM inversion for real data. (A) magnetic integral equation inversion. (B) electric integral equation inversion.

For magnetic permeability inversion, we have developed a new electric integral equation (Li and Xie, 1997),

$$\mathbf{E}(\mathbf{r}) = \mathbf{E}_b(\mathbf{r}) - \int_{V_s} \nabla_{r'} g_b(\mathbf{r}, \mathbf{r}') \times \frac{\mu - \mu_b}{\mu} (\nabla_{r'} \times \mathbf{E} - \mathbf{M})\, d\mathbf{r}' + \int_{V_s} \nabla_r \times \mathbf{G}_s^H(\mathbf{r}, \mathbf{r}') \frac{\mu - \mu_b}{\mu} (\nabla_{r'} \times \mathbf{E} - \mathbf{M})\, d\mathbf{r}', \quad (38)$$

where μ is the magnetic permeability to be defined, μ_b is the background magnetic permeability, $\mathbf{G}_s^H(\mathbf{r}, \mathbf{r}')$ is the background secondary magnetic Green's function, $\mathbf{M}$ is a magnetic source term, $\mathbf{H}_b^E$ is the background magnetic field exited by the electric dipole source, V_s is the scattering integral domain in which $\mu - \mu_b \neq 0$, and σ, ϵ is constant.

The magnetic-field integral equation (8) is dual of the electric integral equation (38) respectively. A new complete EM inversion for σ, ϵ, μ is developed by joining Eqs. (8) and (38) (Xie et al., 1996c). Historically, the approaches for the forward problem and the inverse problem were developed independently of each other. In general, the matrix of the forward problem is sparse and well-posed when the differential equation is discretized by the finite-element or the finite-difference method, but require artificial radiating or absorbing boundary conditions. A merit of the integral-equation method for inversion is that the artificial boundary condition is not needed, but the matrix is full. Coupling integral and differential methods through a domain decomposition gives a local sparse matrix in which boundary conditions are handled by the integral equation.

Acknowledgments

The new 3-D nonlinear magnetic integral inversion algorithm is supported by the Office of Basic Energy Sciences, VETEM program, Engineering and Geosciences Division, Office of Technology Development, and the Office of Oil, Gas and Shale Technologies, Fossil Energy Division, of the U.S. Department of Energy under Contract No. DE-AC03-76SF00098 and DOE Massively Parallel computer allocation. The authors would like to thank Dr. Bruce Curtis and consultants of the National Energy Research Supercomputer Center, and Carol Taliaferro for their help.

References

Golub, G. H., and Van Loan, C. F., 1989, Matrix computations: Johns Hopkins Univ. Press.

Habashy, T. M., Groom, R. W., and Spies, B. R., 1993, Beyond the Born and Rytov approximation: J. Geophys. Res., **98**, no. B2, 1759–1775.

Lee, K. H., and Xie, G., 1995, Electrical and EM methods for high-resolution subsurface imaging: 3rd Soc. Expl. Geophys. Jap./Soc. Expl. Geophys. Internat. Symposium on Geotomography.

Lee, K. H., Xie, G., Hoversten, M., and Pellerin, L., 1995, EM imaging for environmental site characterization: Internat. Symposium on Three-Dimensional Electromagnetics, Schlumberger-Doll Research.

Li, J., Lee, K. H., Javandel, I., and Xie, G., 1995, Nonlinear three-dimensional inverse imaging for direct current data: 65th Annual Internat. Mtg. Soc. Expl. Geophys., Expanded Abstracts, 250–253.

Li, J., and Xie, G., 1997, A new 3D magnetic permeability inversion: Lawrence Berkeley National Laboratory Report.

Tikhonov, A. N., and Arsenin, V. Y., 1977, Solutions to ill-posed problems: John Wiley & Sons, Inc.

Torres-Verdin, C., and Habashy, T. M., 1994, Rapid 2.5-D forward modeling and inversion via a new nonlinear scattering approximation: Radio Sci., **29**, 1051–1079.

Varga, R. S., 1962, Matrix iterative analysis: Prentice–Hall, Inc.

Wilkinson, J. H., 1965, The algebraic eigenvalue problem: Clarendon Press.

Xie, G., Li, J., and Chen, Y. M., 1987, Gauss-Newton-regularizing method for solving coefficient inverse problem of PDE and its convergence: J. Comput. Math., **5**, 38–49.

Xie, G., and Zou, Q., 1991, A parallel algorithm for solving the 3-D inverse scattering problem: Comput. Phys. Commun., **65**, 320–326.

Xie, G., and Lee, K. H., 1995, Nonlinear inversion of 3-D electromagnetic data, *in* Progress in Electromagnetics Research Symposium, Proc., Univ. of Washington, 323.

Xie, G., Lee, K. H., and Li, J., 1995c, A new parallel 3-D numerical modeling of the electromagnetic field: 65th Ann. Mtg, Soc. Expl. Geophys., Expanded Abstracts, 821–824.

Xie, G., Li, J., and Lee, K. H., 1995a, New 3-D nonlinear electromagnetic inversion: Internat. Symposium on Three-Dimensional Electromagnetics, Schlumberger-Doll Research, 405–414.

———1995b, Annealing regularization for high resolution geophysical tomography: Proc. of 3rd Internat. Symposium on Geotomography, Soc. Expl. Geophys. Jap./Soc. Expl. Geophys., 102–109.

Xie, G., Lee, K. H., Li, J., Pellerin, L., and Zuo, D., 1996, 3-D fast finite element Born accelerating electromagnetic imaging using integral equation: 66th Ann. Mtg., Soc. Expl. Geophys., Expanded Abstracts, 261–264.

Xie, G., and Li, J., 1997, A new 3-D parallel high resolution electromagnetic nonlinear inversion based on a global integral and local differential decomposition: Lawrence Berkeley National Laboratory Report, LBNL-40265.

Yagola, A. G., 1980, On the choice of regularization parameter when solving ill-posed problems in reflexive spaces: USSR Comput. Math. Math. Phys., **20**, 40–52.